Journal of Solid State Chemistry 184 (2011) 881–887

Contents lists available at ScienceDirect

Journal of Solid State Chemistry

journal homepage: www.elsevier.com/locate/jssc

Photovoltaic properties of graphene oxide sheets beaded with ZnO nanoparticles

Huan Wang [a], Li Wang [a], Chaoqun Qu [a], Yadong Su [a], Shansheng Yu [a], Weitao Zheng [a,*], Yichun Liu [b]

[a] Department of Materials Science, Key Laboratory of Mobile Materials, MOE, and State Key Laboratory of Superhard Materials, Jilin University, Changchun 130012, People's Republic of China

[b] Center for Advanced Optoelectronic Functional Materials Research, and Key Laboratory for UV-Emitting Materials and Technology of Ministry of Education, Northeast Normal University, 5268 Renmin Street, Changchun 130024, People's Republic of China

ARTICLE INFO

Article history:
Received 23 August 2010
Received in revised form
15 February 2011
Accepted 22 February 2011
Available online 26 February 2011

Keywords:
Photocurrent
Photovoltage
Graphene oxide
Composite

ABSTRACT

A hybrid material of graphene oxide (GO) sheets beaded with ZnO nanoparticles was prepared. The material extends over a few hundred square nanometers, in which the ZnO nanoparticles (average diameter (~5 nm)) are dispersed evenly on the GO sheet. Both the surface photovoltage or surface photocurrent intensity for the material are much stronger than for pure ZnO nanoparticles, meaning that the free charge carriers can effectively be transferred from ZnO nanoparticles to GO sheets, which can serve as a probe to monitor the electron transfer from excited ZnO to GO. Anchoring ZnO nanoparticles on two dimensional carbon nanostructures such as GO can pave a way towards the design of ordered nanostructure assemblies that can harvest light energy efficiently.

1. Introduction

Graphene is a flat monolayer of sp^2 carbon atoms tightly packed into a two- dimensional (2-D) honeycomb lattice, which has attracted a great deal of attention due to its remarkable electronic and structural properties [1–3]. Recently, graphene is used as a new nanomaterial with different device applications, such as field-effect transistors [4,5], resonators [6], transparent anodes [7], supercapacitor devices [8], lithium-ion batteries [9], organic photovoltaic (PV) devices [10], biophysics area [11], etc. With this in mind, the mechanical or chemical exfoliation, epitaxial growth on silicon carbide or metal surfaces, and chemical reduction of dispersed GO have been developed for preparing graphene sheets [12]. GO is an oxidized form of graphene, decorated by hydroxyl and epoxy functional groups on the hexagonal network of carbon atoms with carboxyl groups at the edges [13]. It has been recognized that the reduced GO differs significantly from its pristine, defect-free counterpart, which is usually produced by the micromechanical cleavage of bulk graphite [14]. Recently, a lot of efforts have been devoted to the design and controlled fabrication of composites or hybrid materials which integrate GO or reduced GO with polymers, nanoparticles, or even nanotubes and fullerenes. Functionalization of graphene with different molecules is a powerful chemical route to tailor its properties. Thus, changes in properties brought about by molecular charge transfer could be used for certain applications [15]. For example, Liu et al. [16] have reported PV devices with bulk heterojunction structure using an organic solution processable functionalized graphene material as electron-accepter material and poly(3-hexylthiophene) and poly(3-octylthiop-hene) as donor material. Kamat [17] has developed graphene-based nanoarchitectures with reduced graphene oxide is used as a support to anchor semiconductor (TiO_2, ZnO) and metal nanoparticles (Au, Pt), provided a simple and attractive approach toward designing next-generation catalyst systems. Under UV irradiation, photocatalytically active semiconductor nanoparticles, such as TiO_2 [18–21], ZnO [22,23], $BiVO_4$ [24], have reduced GO into RGO sheets, and graphene-based composite as high performance photocatalysts and facilitate their application in the environmental protection issues.

PV cells containing semiconductor nanocrystals as active materials have been studied extensively [25–27]. Based on the extremely large surface areas of the nanocrystals, combined with their deliberate engineering of the energy-band alignment, it is possible to obtain nanoscale PV devices with excellent performance [28]. Also, the efficiency enhancement of charge separation and transfer in the composites can play a very important role in improving PV response. Li et al. [29] have reported that employing an ensemble of ZnO quantum dot-carbon nanotube (ZnO QD-CNT) heterostructures as PV devices has achieved high charge separation and transfer efficiency. Since GO sheets can also play a similar role of providing unique 2-D architecture to support semiconductor ZnO nanoparticles, reported recently [23], we expect that GO–ZnO hybrids nanoparticles composite can be

* Corresponding author. Fax: +431 85168246.
E-mail address: wtzheng@jlu.edu.cn (W. Zheng).

0022-4596/$ - see front matter © 2011 Elsevier Inc. All rights reserved.
doi:10.1016/j.jssc.2011.02.025

utilized to improve PV response, compared to ZnO nanoparticles. Motivated by this expectation, in this work, anchored ZnO nanoparticles onto a few layers of GO sheets have been prepared by a very simple and straightforward process. The surface photovoltage (SPV) method is a well established contactless and nondestructive technique for semiconductor characterization that relies on analyzing illumination-induced changes in the surface voltage. An SPV arises whenever light induced excess charge carriers are separated in the surface space charge region. Therefore, the formation of an SPV signal is determined by the fundamental properties of light absorption and transport of excess carriers in a semiconducting material [30]. It has been utilized as an extensive source of surface and bulk information on various semiconductors and semiconductors interface. For a semiconductor, electron–hole pairs can be generated under the band gap illumination. These photogenerated electrons (holes) can react with acceptors (donors) adsorbed on the surface of the semiconductor, which results in the change of conductance of the material.

Under UV irradiation, the influence of GO sheet on the separation of photogenerated electron–hole pairs has been investigated by means of surface photovoltage (SPV) and surface photocurrent (SPC). The electron transfer between the semiconductor ZnO nanoparticles and GO sheets has also been studied. This investigation indeed indicates that there may be a potential practical application for GO–ZnO hybrids composites in PV devices [31].

2. Experimental

The starting materials used in the experiments were natural graphite (99 wt% purity, Oingdao Yingshida Graphite Co. Ltd), $NaNO_3$ (Tianjin Guangfu Chemicals Co., Ltd), H_2SO_4 (98 wt%, analytical reagent = A. R., Beijing Beihua Chemicals Co., Ltd), H_2O_2 (30 wt%, A. R., Beijing Beihua Chemicals Co., Ltd), HCl (37 wt%, A. R., Beijin Beihua Chemicals Co., Ltd), $Zn(CH_3COO)_2 \cdot 2(H_2O)$ (99 .99 wt.%, A. R., M0FF0C; Beijing Beihua Chemicals Co., Ltd), $Li(OH) \cdot (H_2O)$ (99.99 wt.%, A. R., Beijing Beihua Chemicals Co., Ltd), *N*, *N*-dimethylformamide (DMF, 98 wt.%, A. R., Tianjin Fuyu Chemicals Co., Ltd), Hydeazine hydrate (80 wt%, A. R., Tianjin Fuyu Chemicals Co., Ltd) and ethanol (99 wt%, A. R., Beijing Beihua Chemicals Co., Ltd).

2.1. Synthesis of GO

GO was prepared using a modified Hummers method from graphite powders [32,33]. $NaNO_3$ (1.5 g) was mixed with concentrated sulfuric acid (67.5 ml) at room temperature. Then natural graphite (2.0 g) was added to the solution while stirring, this mixture was cooled to 0 °C in an ice bath, followed by slow addition of 9.0 g $KMnO_4$, and the reaction mixture was allowed to stand for five days at room temperature with stirring. On completion of the reaction, 100 mL of 5 wt% H_2SO_4 aqueous solution was added to the mixture over about 1 h with stirring for 2 h. Then 6 mL of H_2O_2 (30 wt% aqueous solution) was added to the above liquid and the mixture was stirred for 2 h at room temperature. Finally, the resulting suspension was filtered, washed with a mixed aqueous solution of 3 wt% H_2SO_4/0.5 wt% H_2O_2 and water, and dried at room temperature for 24 h to obtain GO sheets.

2.2. Preparation of ZnO nanoparticles

ZnO nanoparticles were synthesized by directly mixing zinc acetate and lithium hydroxide in ethanol with sonication [34]. Firstly, $Zn(Ac)_2 \cdot 2H_2O$ (220 mg) was dissolved in ethanol (50 ml) with sonication for 10 min at 0 °C. Then $Li(OH) \cdot H_2O$ (42 mg) was added and sonication continued for another 10 min at 0 °C. A stable and optically transparent ZnO colloidal suspension was prepared by this method. Hexane (100 ml) was added to ZnO suspension so that particles were precipitated out of the solution, precipitates were dried at room temperature for 12 h.

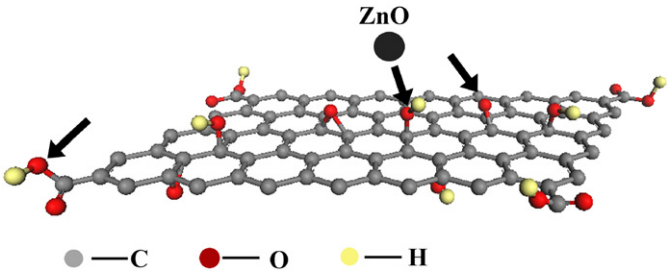

Fig. 1. Formation process of GO–ZnO hybrid composite.

2.3. Preparation of GO–ZnO hybrids composites

GO (50 mg) in DMF solvent (10 ml) and ZnO precipitate in DMF solvent (40 ml) were dispersed by sonication separately. The two colloidal suspensions were then mixed together with vigorous stirring; the solution was heated in a water bath at 90 °C for 5 h. We observed that the suspension gradually evolved into a brown-bark solution. The final products were then centrifuged, washed, and finally dried. In GO suspension, these oxy-functional groups had more affinity to Zn element in ZnO nanoparticles. The formation of GO–ZnO hybrid composite was due to the adsorption of ZnO nanoparticles on GO sheets surface at 90 °C, as shown in Fig. 1 [35].

2.4. Characterizations

X-ray diffraction (XRD) of the powder samples was performed to investigate the structure of samples, using a Bragg-Brentano diffractometer (D8_tools) in θ–2θ configuration with a Cu $K\alpha$ line at 0.15418 nm as a source, while an atomic force microscope (AFM, Seiko Instruments Industry, Co. Ltd. SPA300HV with an SPI 3800 controller) and transmission electron microscope (TEM, Hitachi H-8100) and high-resolution TEM (HRTEM) (JOEL TEM-2010) with a field emission gun operating at 160 kV were employed to inspect the morphologies for samples. Absorption spectra measurements were carried out using a Shimadzu UV-3150 spectrometer at room temperature, whereas Raman spectra measurements were operated using a LabRam HR-800 confocal Raman microscope in which 488 and 325 nm laser were employed as the light source. The SPC and SPV spectra measurements were performed using a lock-in based surface photovoltaic spectroscopy (SPS) measurement system [36]. The SPS measurement system is constituted of a source of monochromatic light, a lock-in amplifier (SR830-DSP) with a light chopper (SR540), a photovoltaic cell, and a computer. A 500 W xenon lamp and a double-prism monochromator provide monochromatic light. A low chopping frequency of ~30 Hz is used.

3. Results and discussion

3.1. Formation and morphology of the GO–ZnO hybrids composites

Fig. 2 shows the XRD patterns of the natural graphite powder (a), as-prepared GO samples (b), and GO–ZnO hybrids composites (c), wherein a very strong (0 0 2) peak at 26.54° (Fig. 2(a)) appears for the natural graphite powder displays, indicating a typical pattern of crystal graphitic structure with a layer-layer distance (d-spacing) of 0.334 nm. After oxidation, the interlayer spacing of d_{002} becomes large (0.84835 nm) (Fig. 2(b)), much larger than that of graphite. The increased d-spacing for GO sheets can be ascribed to oxide-induced

O-containing groups such as carboxyl (–COOH), hydroxyl (–OH), and epoxy groups, inserted H_2O molecules, and other structural defects [37]. Fig. 2(c) shows that ZnO particles spread on the GO sheets form a hexagonal structure and have major peaks at around (2θ) 31.4° (100), 35.9° (101), 47.4° (102), and 56.3° (110). In general, the nanocrystallite size can roughly be estimated from the Scherrer formula: $D_{hkl}=K\lambda/(\beta\cos\theta)$, where λ is the X-ray wavelength (0.15418 nm), β the full-width at half-maximum, θ the diffraction angle, K a constant (0.89) and D_{hkl} means the size along (h k l) direction [38]. Here we take diffraction data along all the planes to roughly calculate the size of the nanocrystallites, and the roughly estimated average crystallite sizes of ZnO nanoparticles is around 7 nm on the surface of GO sheets, which is in good agreement with TEM results, discussed in the following.

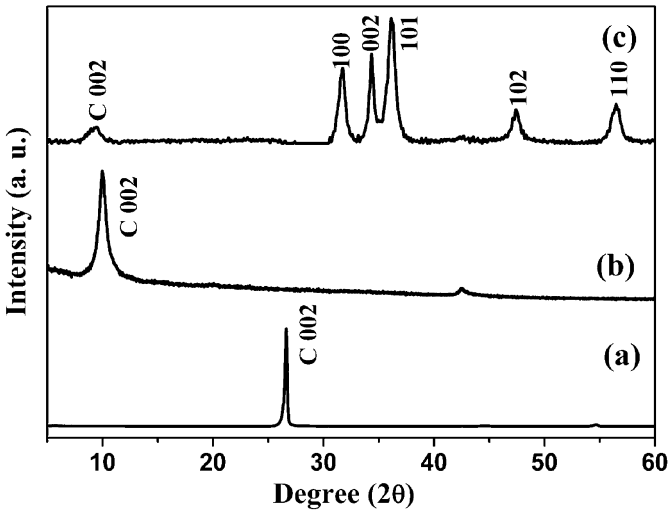

Fig. 2. X-ray diffraction patterns for the natural graphite powder (a), GO (b), and GO–ZnO hybrid composite (c), wherein the Miller indices of diffracting lattice planes are indexed.

Fig. 3 exhibits the AFM images and line profiles of as-prepared GO sheets (Fig. 3(a), (b)) and GO–ZnO hybrids composites (Figs. 3(c), (d)), respectively. In both cases, the lateral dimensions of sheets range from a few hundred nanometers to about 1 μm. A typical cross-section image of as-prepared GO sheets (Fig. 3(b)) indicates an average thickness of 2.0 nm, consistent with the characteristic value of two layer sheets reported in the literature [14]. In the case of GO–ZnO hybrids composites, we find that the thickness (4–5 nm) is not uniform because of the coating of ZnO particles (Fig. 3(b)).

In order to reveal the microstructure for as-prepared GO sheets and GO–ZnO hybrid composite, TEM and HRTEM measurements are performed, and the results are shown in Fig. 4. From TEM image of as-prepared GO sheets (Fig. 4(a)), large sheets (a few hundred square nanometers) resemble waved silk veils. They were transparent and entangled with each other. Fig. 4(b) and (c) shows the TEM images of the GO–ZnO hybrid composite, having two different magnifications, in which above-mentioned sheet conjugations are also clearly observed. The average diameter (~5 nm) of the ZnO nanoparticles on the GO sheets is estimated from the TEM images (Fig. 4(b) and (c)). Fig. 4(d) displays the HRTEM image of the GO–ZnO hybrids composites, in which there exist a few nanocrystal particles on the GO sheet. In the crystalline regions indicated by white arrows (Fig. 4(d)), the distance (0.2868 nm) between the adjacent lattice fringes just corresponds to the interplanar distance of ZnO (1 0 0) planes, agreeing well with the d (1 0 0) spacing (0.2814 nm) (JCPDS No. 36-1454) in the literature, which does not correspond to none of the interplanar distance of graphitic lattice. Thus we can judge that the nanocrystals indicated by white arrows are ZnO. It is noteworthy that the structure of region indicated by green boxes (Fig. 4(d)) is different from ZnO. In order to identify the structure, the regions indicated by green boxes are enlarged, as shown in Fig. 4(e), wherein the hexagonal lattice is clearly observed. The structural

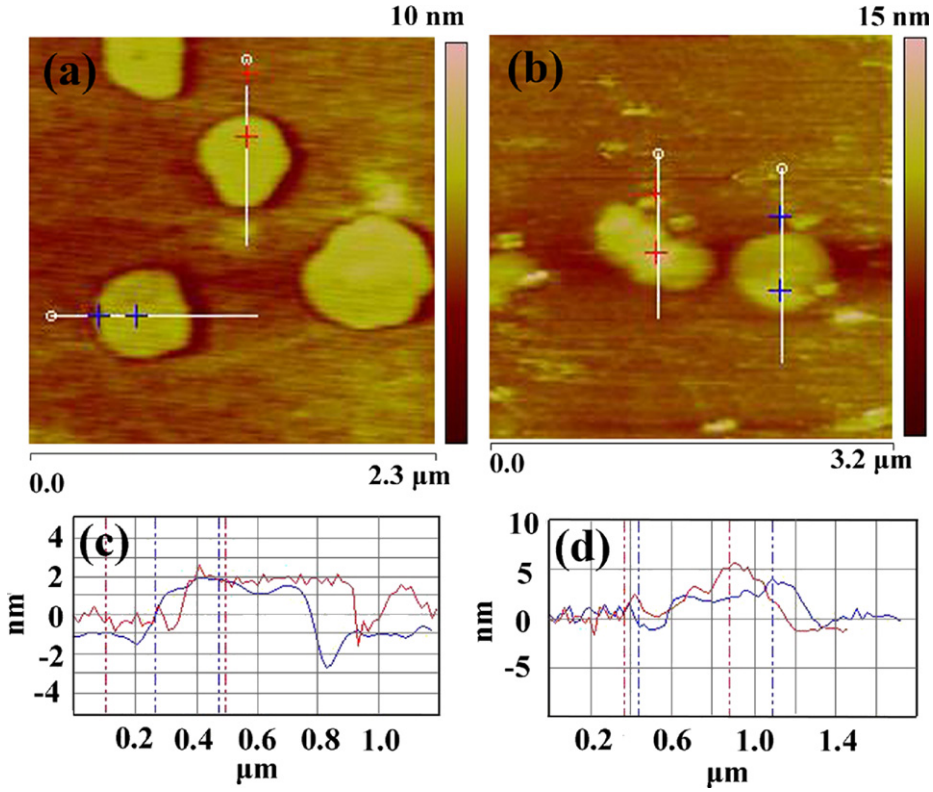

Fig. 3. AFM images with height profile from the as-prepared GO sheets (a, c) and GO–ZnO hybrid composite (b, d), respectively.

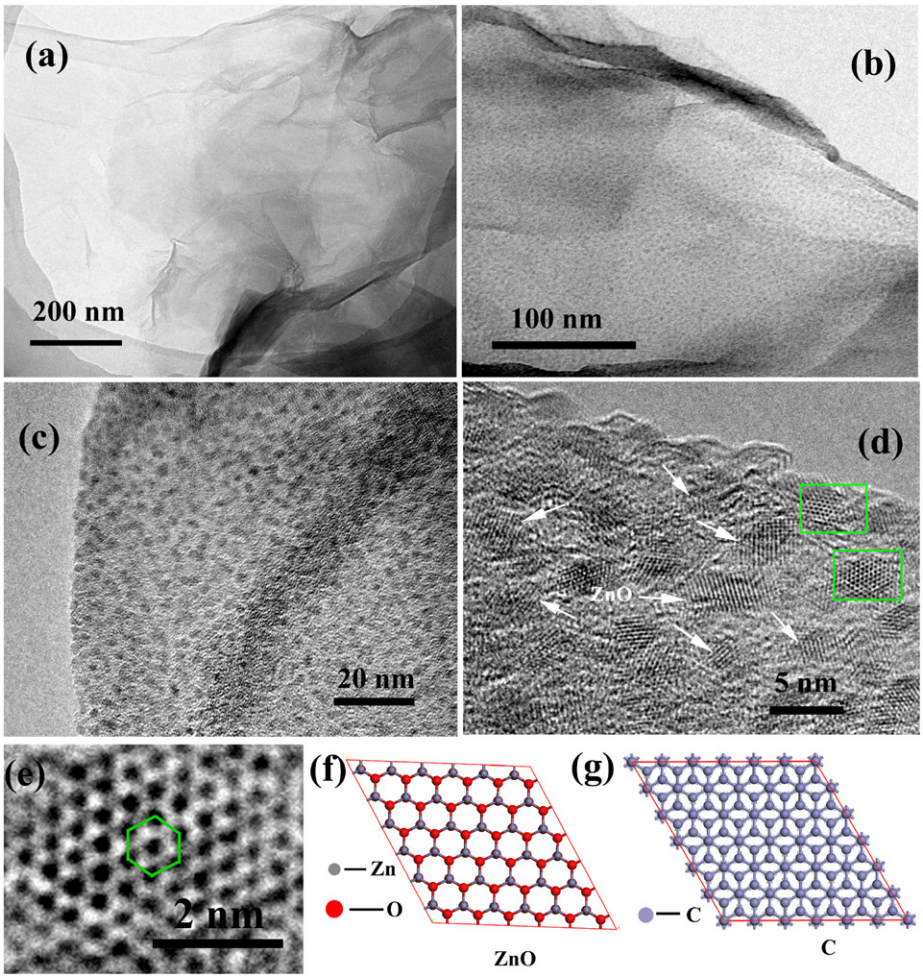

Fig. 4. TEM and high-resolution TEM images for the as-prepared GO sheets (a), GO–ZnO hybrid composite (b–e), structural representation of top view for hexagonal zinc oxide (f) and AB Bernal stacked graphite (g). (For interpretation of the references to color in this figure, the reader is referred to the web version of this article.)

representations of top view for hexagonal zinc oxide and AB Bernal stacked graphite are shown in Fig. 4(f) and (g). By comparing the structural representation of top view of graphite with hexagonal zinc oxide, we can confirm that the hexagonal lattice (in Fig. 4(e)) is due to the corresponding overlapping of neighboring carbon layers in the AB Bernal stacked graphene layers [39].

Raman spectrum measurements are performed at room temperature with different excitation energies at 325 and 488 nm. Fig. 5(a) and (b) shows Raman spectra of the as-prepared GO sheets and the GO–ZnO hybrids composites at 488 nm, respectively. The two intense peaks at 1355 and 1596 cm^{-1} are observed in Fig. 5(a), which correspond to the well documented D and G band [40]. The appearance of the D band signifies disorder in the graphitic lattice, which might be attributed to the some defects induced during the fabrication process or influence originate from the edges of the GO layers [41]. The G peak is due to the doubly degenerate zone center assigned to the E_{2g} phonon mode, while the D line is a breathing mode of κ-point phonons of A_{1g} symmetry [42]. As noticed from the spectrum of the GO–ZnO hybrids composites in Fig. 5(b), the intensity ratio of the G and D band, I_G/I_D, increases and the G peak has a significant red shift in comparison with that of the starting GO material (Fig. 5(a)), which can be attributed to the reaction process that has introduced a graphitic "self-healing" similar to what is observed from the sharpening of the G peak and the intensity decrease of the D peak in heat-treated graphite [43]. I_G/I_D is a measure of the degree of graphitization and I_G/I_D is proportional to the average size of the sp^2 domains, thus the average size of the crystalline graphene domains may be increased in our GO–ZnO sheets [44].

Fig. 5(c) shows the Raman spectrum of GO–ZnO hybrid composite excited by He–Cd laser using 325 nm line. As shown in Fig. 5(c), two LO phonon peaks are observed at 571 cm^{-1} (1LO) and 1142 cm^{-1} (2LO), which illustrates that multiphonon resonant process for ZnO nanoparticles in GO–ZnO samples occurs [45]. In addition, other two peaks at 1405 and 1590 cm^{-1} are also observed, which correspond to the well documented D and G band for graphitic lattice [46,47]. These results further confirm the presence of ZnO nanoparticles spread on GO sheets, agreeing well with the XRD results.

3.2. SPS properties of the GO–ZnO hybrid composites

The UV–vis absorption spectra for ZnO nanoparticles, as-prepared GO sheets and GO–ZnO hybrids composites are shown in Fig. 6, wherein the absorption spectra for ZnO and GO–ZnO exhibit a broad band in the range of 310–350 nm, which can be attributed to the band-band transition of charges in ZnO [48], while the absorption spectrum for as-prepared GO sheets shows no obvious absorption band. In this work, as the ZnO nanoparticles are attached onto the as-prepared GO sheets, the heterojunction between a ZnO nanoparticle and GO sheet is formed. In order to investigate the mechanism of photogenerated charge transfer at the junction between a ZnO nanoparticle and GO sheet, SPV measurements are carried out.

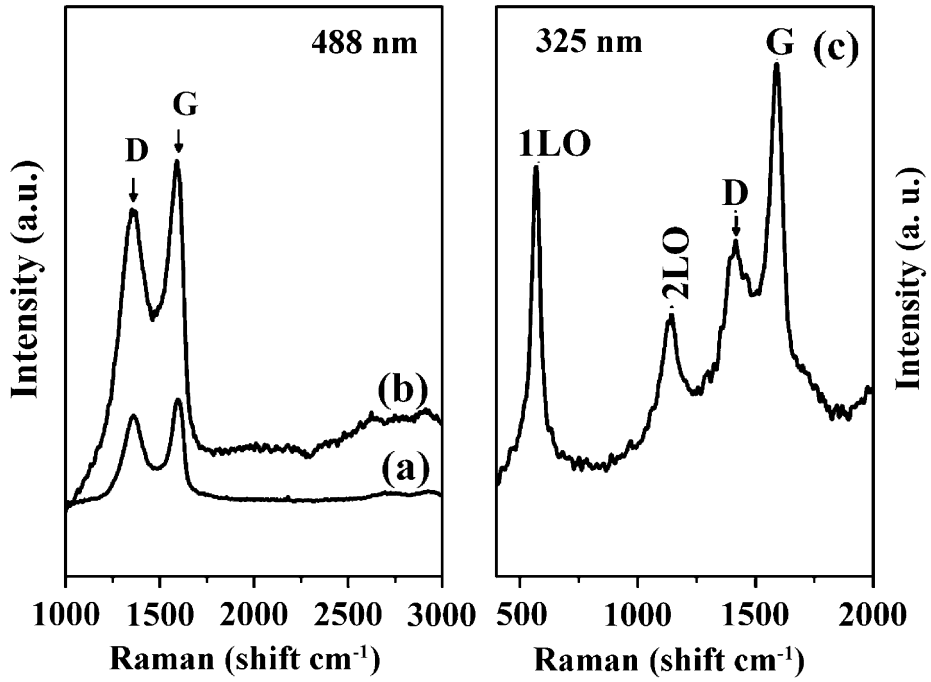

Fig. 5. Raman spectra for the as-prepared GO sheets (a) using 488 nm excitation, and GO–ZnO hybrid composite using (b) 488 nm and (c) 325 nm excitation.

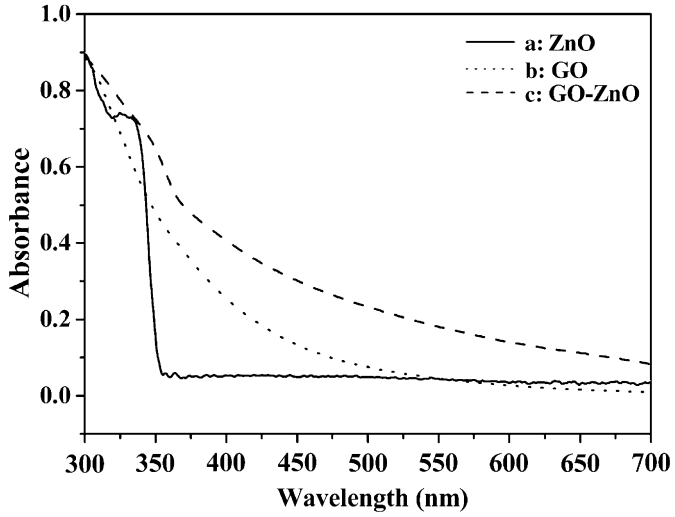

Fig. 6. UV/vis spectra of ZnO (a), GO sheets (b), and GO–ZnO hybrid composite (c).

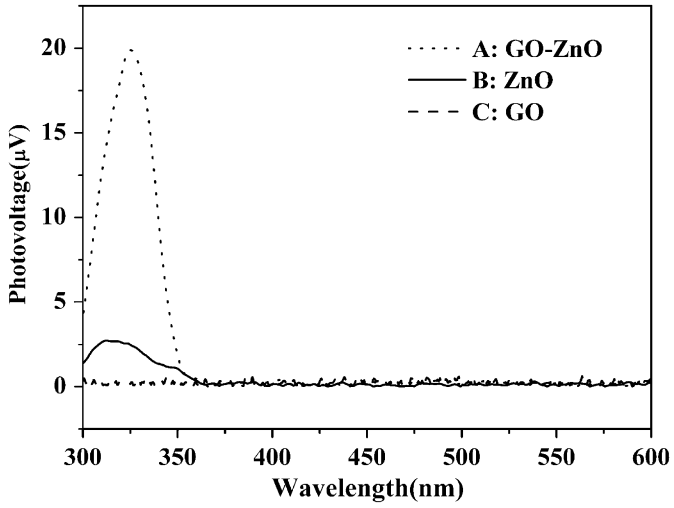

Fig. 7. Surface photovoltage spectra of GO–ZnO hybrid composite (A), ZnO nanoparticles (B), and GO sheets (C).

After absorbing light with a certain wavelength, the electron–hole pairs in sample are generated, the separation of the electron–hole pairs will lead to the formation of the SPV signal. Due to the different diffusion constants of electrons and holes, the concentration gradient of free charge carriers is produced, and the height of the surface potential barrier of the sample is changed [49]. While varying the concentration of accumulated free charge carriers at the surface, SPV intensity will change. Fig. 7 shows the SPV spectra of our obtained ZnO and GO–ZnO samples, in which the SPV spectra only shows a broad band with the maximum value at 325 nm, which is due to the band-to-band transition of charges in ZnO nanoparticles. The SPV intensity for the ZnO nanoparticles is much weaker than the GO–ZnO hybrid composite. For the ZnO nanoparticles, the particle size is so small that the surface effect can come into effect, leading to that the free charge carriers are elastically scattered or quenched by the nanoparticle boundary [50]. Consequently, the photogenerated electron–hole pairs in ZnO nanoparticles cannot be effectively separated, and the ZnO nanoparticles are unable to make a strong SPV response [51].

Fig. 8 shows the schematics of photogenerated charge injected from excited semiconductor particle into GO sheets, and the expected PV mechanism. For GO–ZnO hybrid nanoparticles composite, under short UV irradiation, the photogenerated charge in ZnO nanoparticles transfers from the valence band (VB) to conduction band (CB), and hence charge–hole pairs are produced. This charge transition can be described in the following equation:

$$ZnO + h\nu \rightarrow ZnO(e_{CB} + h_{VB}) \quad (1)$$

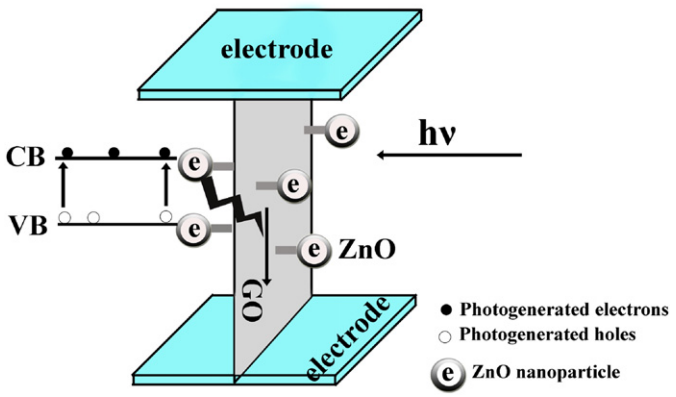

Fig. 8. Photogenerated charge injection from excited semiconductor particle (ZnO) into GO sheet.

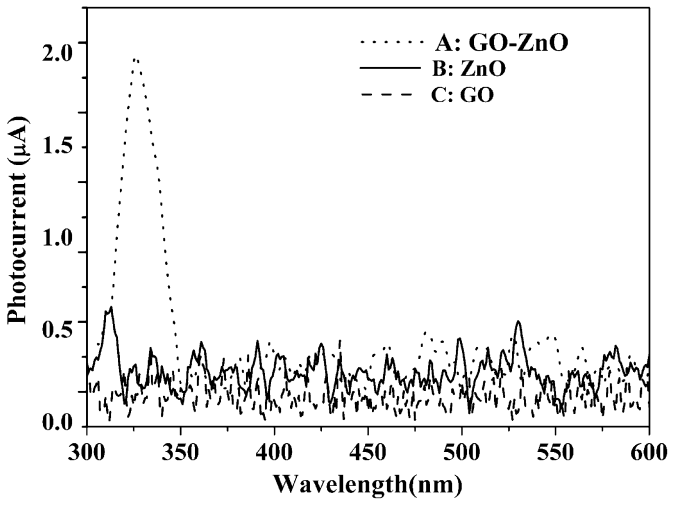

Fig. 9. Surface photocurrent spectra of GO–ZnO hybrid composite (A), ZnO nanoparticles (B), and GO sheets (C).

The interfacial charge transfer process between the excited ZnO particles and GO can be illustrated as below (also see Fig. 2)

$$ZnO(e)+GO \rightarrow ZnO+GO(e) \quad (2)$$

Based on Eq. (2) and Fig. 8, the ZnO nanoparticles attached on the GO sheets could facilitate the transfer of conduction-band electrons from the ZnO nanoparticles to GO sheets, resulting in a charge separation between the ZnO nanoparticles to the GO sheets. Consequently, the intensity of SPV for the GO–ZnO hybrid composite is enhanced. The electron transfer between the ZnO nanoparticles and GO also occurs as the GO–ZnO hybrid composite induces photoluminescence [23]. Since the photogenerated electrons and holes in the vicinity of the GO–ZnO junction can directly be driven by the electric filed, the generated photocurrent can be detected [52]. Fig. 9 displays the SPC spectra of ZnO nanoparticles and GO–ZnO samples. Notably, the current intensity of the GO–ZnO hybrid composite is much higher than that of ZnO nanoparticles. Upon irradiating the GO–ZnO samples with a light having an energy equalizing the band gap energy, the carrier concentration in the GO–ZnO hybrid composite increases sharply, leading to a pronounced increase in the current intensity. However, the photocurrent response of the ZnO nanoparticles cannot be observed, which can be attributed to that the free charge carriers are elastically scattered or quenched by the ZnO nanoparticle boundary.

4. Conclusions

Thin sheet GO and ZnO nanoparticles hybrid composites have been successfully prepared using a very simple and straightforward reaction at 90 °C, in which the GO sheet can be used as support architectures to anchor semiconductor nanoparticles such as ZnO. Upon UV excitation, the generated electron–hole pairs can be separated effectively in the GO–ZnO hybrid composite structure. Both the SPC and SPV spectra confirm that the involvement of the GO scaffold facilitates the charge collection and charge transport in the GO–ZnO hybrid composite. The results presented in this work can pave a way towards the design of ordered nanostructure assemblies that can harvest light energy quite efficiently.

Acknowledgments

The support from National Natural Science Foundation of China (Grant nos. 50525204, 50902057 and 50832001), the special Ph.D. program (Grant no. 200801830025) from MOE, and the “211” and “985” project of Jilin University, China, is highly appreciated.

References

[1] A.K. Geim, K.S. Novoselov, Nat. Mater. 6 (2007) 183–191.
[2] C. Berger, Z.M. Song, X.B. Ni, X.S. Wu, N. Brown, C. Naud, D. Mayou, J. Hass, T.B. Li, A.N. Marchenkov, E.H. Conrad, P.N. First, W.A. de Heer, Science 312 (2006) 1191–1196.
[3] J. Nilsson, A.H.C. Neto, F. Guinea, N.M.R. Peres, Phys. Rev. Lett. 97 (2006) 266801.
[4] F. Schedin, A.K. Geim, S.V. Morozov, E.W. Hill, P. Blake, M.I. Katsnelson, K.S. Novoselov, Nat. Mater. 6 (2007) 652–655.
[5] F. Chen, Q. Qing, J.L. Xia, J.H. Li, N.J. Tao, J. Am. Chem. Soc. 131 (2009) 9908–9909.
[6] K.S. Novoselov, A.K. Geim, S.V. Morozov, D. Jiang, Y. Zhang, S.V. Dubonos, I.V. Grigorieva, A.A. Firsov, Science 306 (2004) 666–669.
[7] X. Wang, L.J. Zhi, K. Müllen, Nano Lett. 8 (2008) 323–327.
[8] Y. Wang, Z.Q. Shi, Y. Huang, Y.F. Ma, C.Y. Wang, M.M. Chen, Y.S. Chen, J. Phys. Chem. C 113 (2009) 13103–13107.
[9] E.J. Yoo, J. Kim, E. Hosono, H. Zhou, T. Kudo, I. Honma, Nano Lett. 8 (2008) 2277–2282.
[10] Q. Liu, Z.F. Liu, X.Y. Zhang, N. Zhang, L.Y. Yang, S.G. Yin, Y.S. Chen, Appl. Phys. Lett. 92 (2008) 223303.
[11] O. Akhavan, E. Ghaderi, ACS Nano. 4 (2010) 5731–5736.
[12] Y.Y. Liang, D.Q. Wu, X.L. Feng, K. Müllen, Adv. Mater. 21 (2009) 1–5.
[13] G.K. Ramesha, S. Sampath, J. Phys. Chem. C 113 (2009) 7985–7989.
[14] J.I. Paredes, S. Villar-Rodil, P. Solis-Fernandez, A. Martinez-Alonso, J.M.D. Tascon, Langmuir 25 (2009) 5957–5968.
[15] C.N.R. Rao, A.K. Sood, R. Voggu, K.S. Subrahmanyam, J. Phys. Chem. Lett. 1 (2010) 572–580.
[16] Z.F. Liu, Q. Liu, Y. Huang, Y.F. Ma, S.G. Yin, X.Y. Zhang, W. Sun, Y.S. Chen, Adv. Mater. 20 (2008) 3924–3930.
[17] P.V. Kamat, J. Phys. Chem. Lett. 1 (2010) 520–527.
[18] O. Akhavan, E. Ghaderi, J. Phys. Chem. C 113 (2009) 20214–20220.
[19] H. Zhang, X.J. Lv, Y.M. Li, Y. Wang, J.H. Li, ACS Nano 4 (2010) 380–386.
[20] T.N. Lambert, C.A. Chavez, B. Hernandez-Sanchez, P. Lu, N.S. Bell, A. Ambrosini, T. Friedman, T.J. Boyle, D.R. Wheeler, D.L. Huber, J. Phys. Chem. C 113 (2009) 19812–19823.
[21] Y.H. Ng, I.V. Lightcap, K. Goodwin, M. Matsumura, P.V. Kamat, J. Phys. Chem. Lett. 1 (2010) 2222–2227.
[22] J.M. Lee, Y.B. Pyun, J. Yi, J.W. Choung, W.I. Park, J. Phys. Chem. C 113 (2009) 19134–19138.
[23] G. Williams, P.V. Kamat, Langmuir 25 (2009) 13869–13873.
[24] Y.H. Ng, A. Iwase, A. Kudo, R. Amal, J. Phys. Chem. Lett. 1 (2010) 2607–2612.
[25] Y. Wu, C. Wadia, W.L. Ma, B. Sadtler, A.P. Alivisatos, Nano Lett. 8 (2008) 2551–2555.
[26] Z.Q. Liang, K.L. Dzenis, J. Xu, Q. Wang, Adv. Funct. Mater. 16 (2006) 542–548.
[27] I. Gur, N.A. Fromer, C.P. Chen, A.G. Kanaras, A.P. Alivisatos, Nano Lett. 7 (2007) 409–414.
[28] D.I. Son, S.H. Cho, T.W. Kim, Nanotechnology 20 (2009) 085202.
[29] F.S. Li, S.H. Cho, D.I. Son, T.W. Kim, S.K. Lee, Y.H. Cho, S.H. Jin, Appl. Phys. Lett. 94 (2009) 111906.
[30] Q.D. Zhao, T.F. Xie, L.L. Peng, Y.H. Lin, P. Wang, L. Peng, D.J. Wang, J. Phys. Chem. C 111 (2007) 17136–17145.
[31] Q.D. Zhao, M. Yu, T.F. Xie, L.L. Peng, P. Wang, D.J. Wang, Nanotechnology 19 (2008) 245706.
[32] H.A. Becerril, J. Mao, Z.F. Liu, R.M. Stoltenberg, Z.N. Bao, Y.S. Chen, ACS Nano 2 (2008) 463–470.

[33] W.S. Hummers, R.E. Offeman, J. Am. Chem. Soc. 80 (1958) 1339–1339.
[34] F. Vietmeyer, B. Seger, P.V. Kamat, Adv. Mater. 19 (2007) 2935–2940.
[35] K. Jasuja, V. Berry, ACS Nano 3 (2009) 2358–2366.
[36] P. Wang, D.J. Wang, H.Y. Li, T.F. Xie, H.Z. Wang, Z.L. Du, J. Coll. Inter. Sci. 314 (2007) 337–340.
[37] D.Y. Pan, S. Wang, B. Zhao, M.H. Wu, H.J. Zhang, Y. Wang, Z. Jiao, Chem. Mater. 21 (2009) 3136–3142.
[38] J.M. Nedelec, D. Avignant, R. Mahiou, Chem. Mater. 14 (2002) 651–655.
[39] J.H. Warner, M.H. Rümmeli, T. Gemming, B. Büchner, G.A.D. Briggs, Nano Lett. 9 (2009) 102–106.
[40] A. Dato, V. Radmilovic, Z.H. Lee, J. Phillips, M. Frenklach, Nano Lett. 8 (2008) 2012–2016.
[41] D.C. Wei, Y.Q. Liu, H.L. Zhang, L.P. Huang, B. Wu, J.Y. Chen, G. Yu, J. Am. Chem. Soc. 131 (2009) 11147–11154.
[42] K.N. Kudin, B. Ozbas, H.C. Schniepp, R.K. Prud'homme, I.A. Aksay, R. Car, Nano Lett. 8 (2008) 36–41.
[43] G. Compagninia, L. D'Ursoa, O. Puglisia, G.A. Barattab, G. Strazzullab, Carbon 47 (2009) 1605–1612.
[44] C. Gómez-Navarro, R.T. Weitz, A.M. Bittner, S. Matteo, A. Mews, M. Burghard, K. Kern, Nano Lett. 7 (2007) 3499–3503.
[45] Y.W. Zhu, H.I. Elim, Y.L. Foo, T. Yu, Y.J. Liu, W. Ji, J.Y. Lee, Z.X. Shen, A.T.S. Wee, J.T.L. Thong, C.H. Sow, Adv. Mater. 18 (2006) 587–592.
[46] H. Chen, S.L. Gu, W. Liu, S.M. Zhu, Y.D. Zheng, J. Appl. Phys. 104 (2008) 113511.
[47] J. Khanderi, R.C. Hoffmann, A. Gurlob, J.J. Schneider, J. Mater. Chem. 19 (2009) 5039–5046.
[48] G.Y. Shan, S. Wang, X.F. Fei, Y.C. Liu, G.L. Yang, J. Phys. Chem. B 113 (2009) 1468–1472.
[49] Y.H. Lin, D.J. Wang, Q.D. Zhao, Z.H. Li, Y.D. Ma, M. Yang, Nanotechnology 17 (2006) 2110–2115.
[50] C.Q. Sun, Prog. Solid State Chem. 35 (2007) 1–159.
[51] Y.H. Lin, D.J. Wang, Q.D. Zhao, M. Yang, Q.L. Zhang, J. Phys. Chem. B 108 (2004) 3202–3206.
[52] K. Xiao, Y. Fu, Y.Q. Liu, G. Yu, J. Zhai, L. Jiang, W.P. Hu, Z.G. Shuai, Y. Luo, D.B. Zhu, Adv. Funct. Mater. 17 (2007) 2842–2846.